Atmospheric Environment 169 (2017) 204–217

Contents lists available at ScienceDirect

Atmospheric Environment

journal homepage: www.elsevier.com/locate/atmosenv

Evaluation of a multi-scale WRF-CAM5 simulation during the 2010 East Asian Summer Monsoon

Patrick Campbell [a], Yang Zhang [a, e, *], Kai Wang [a], Ruby Leung [b], Jiwen Fan [b], Bo Zheng [c], Qiang Zhang [d], Kebin He [c, e]

[a] Department of Marine, Earth, and Atmospheric Sciences, NCSU, Raleigh, NC, USA
[b] Atmospheric Sciences and Global Change Division, Pacific Northwest National Laboratory, Richland, WA, USA
[c] State Key Joint Laboratory of Environment Simulation and Pollution Control, School of Environment, Tsinghua University, Beijing, China
[d] Ministry of Education Key Laboratory for Earth System Modeling, Center for Earth System Science, Tsinghua University, Beijing, China
[e] Collaborative Innovation Center for Regional Environmental Quality, Beijing, China

HIGHLIGHTS

- WRF-CAM5 adequately predicts meteorology and chemistry down to 4 km resolution.
- Overall good model performance for rain, but issues with convective vs. grid-scale rain.
- Model performance for rain improves with increasing horizontal resolution to 4 km.
- Widespread underpredictions in surface and column aerosol concentrations.
- WRF-CAM5 is limited for regional-scale applications of aerosol-cloud interactions.

ARTICLE INFO

Article history:
Received 2 December 2016
Received in revised form
29 August 2017
Accepted 3 September 2017
Available online 8 September 2017

Keywords:
WRF-CAM5
Online-coupled
Multiple nested
Evaluation
East Asian Summer Monsoon

ABSTRACT

The Weather Research and Forecasting model with Chemistry (WRF-Chem) with the physics package of the Community Atmosphere Model Version 5 (CAM5) has been applied at multiple scales over Eastern China (EC) and the Yangtze River Delta (YRD) to evaluate how increased horizontal resolution with physics designed for a coarser resolution climate model impacts aerosols and clouds, and the resulting precipitation characteristics and performance during the 2010 East Asian Summer Monsoon (EASM). Despite large underpredictions in surface aerosol concentrations and aerosol optical depth, there is good spatial agreement with surface observations of chemical predictions, and increasing spatial resolution tends to improve performance. Model bias and normalized root mean square values for precipitation predictions are relatively small, but there are significant differences when comparing modeled and observed probability density functions for precipitation in EC and YRD. Increasing model horizontal resolution tends to reduce model bias and error for precipitation predictions. The surface and column aerosol loading is maximized between about 32°N and 42°N in early to mid-May during the 2010 EASM, and then shifts north while decreasing in magnitude during July and August. Changing model resolution moderately changes the spatiotemporal relationships between aerosols, cloud properties, and precipitation during the EASM, thus demonstrating the importance of model grid resolution in simulating EASM circulation and rainfall patterns over EC and the YRD. Results from this work demonstrate the capability and limitations in the aerosol, cloud, and precipitation representation of WRF-CAM5 for regional-scale applications down to relatively fine horizontal resolutions. Further WRF-CAM5 model development and application in this area is needed.

© 2017 Elsevier Ltd. All rights reserved.

1. Introduction

Regional climate modeling studies show that the intensity and distribution of precipitation during the East Asian summer monsoon (EASM) is strongly impacted by a combination of both

* Corresponding author. Department of MEAS, NCSU, Campus Box 8208, Raleigh, NC 27695-8208, USA.
E-mail address: yang_zhang@ncsu.edu (Y. Zhang).

http://dx.doi.org/10.1016/j.atmosenv.2017.09.008
1352-2310/© 2017 Elsevier Ltd. All rights reserved.

radiative (direct) and microphysical (indirect) effects of aerosols (Huang et al., 2007; Wu et al., 2013; Lim et al., 2014). The EASM is a sub-system of the larger Asian summer monsoon that brings warm moist air from the Indian and Pacific Oceans over East Asia, resulting in a seasonal and northward progression of heavy precipitation that affects about one third of the world's population (Yihui and Chan, 2005). The EASM precipitation exerts a strong influence on the societal and economic activity of eastern China (EC), in particular over the rapidly developing city of Shanghai. The EASM precipitation exhibits significant variability on intraseasonal, interannual, and multidecadal time scales. For example, a westward shift in the West Pacific Subtropical High and an intense La Niña phase in the Pacific Ocean led to a warmer sea surface in the western Pacific, positive precipitation anomalies, and devastating floods in China during the 2010 EASM (Mujumdar et al., 2012).

With the exception of intense dust storms, the composition and radiative effects of aerosols over the developing regions of EC and the Yangtze River Delta (YRD) are dominated by sources of anthropogenic origin, and are mainly composed of sulfate (SO_4^{2-}) and organic compounds (Xu et al., 2002). Rapid economic development in China has led to further increases in both primary and secondary anthropogenic aerosol emissions (Ohara et al., 2007; Lei et al., 2011), and consequently observations show high aerosol number concentrations over EC and the YRD city-cluster (Cheng et al., 2013; Ding et al., 2013). Ding et al. (2013) showed that over a 1-year period, about 40% of the 24-hr average fine particulate matter ($PM_{2.5}$) concentrations measured at the Xianlin site in YRD exceeded the National Ambient Air Quality Standards in China (75 μg m^{-3}). The YRD city-cluster includes China's largest city of Shanghai, as well as other developing economic centers such as Nanjing, Suzhou, Hangzhou, and Ningbo.

With periods of such high aerosol loading over Asia, aerosol effects (direct + indirect) may have a significant influence on the Asian monsoon circulation and precipitation. Lau and Kim (2006) showed that the direct radiative forcing of absorbing aerosols can produce an elevated heat pump effect, which altered the monsoon strength in South Asia. A combination of remote sensing and radiative transfer modeling confirmed that aerosols can effectively reduce shortwave radiation during the Asian pre-monsoon season by about 20–30 W m^{-2} on a seasonal average, although this shortwave reduction was shown to have a minimal impact on the large-scale monsoonal flow patterns (Kuhlmann and Quaas, 2010). Long-term data analysis combined with cloud-resolving modeling showed that the high aerosol concentrations in EC leads to a spatially coherent increase in cloud droplet number concentrations (CDNCs), which reduces the light rain in EC over the past 50 years (Qian et al., 2009).

There is continued interest in studying the connections between aerosols and the EASM using coupled meteorological-chemical simulations. Table 1 shows a list of coupled models' system, period, type (online vs. offline), domain(s), vertical and horizontal resolutions, major chemistry and aerosol treatments, cloud microphysics, cumulus parameterizations, aerosol activation treatment (i.e., aerosol-cloud interactions), and what (if any) aerosol direct, semidirect, indirect, or total (direct + indirect) effects were investigated for previous studies of aerosol and East Asian climate interactions compared to our work (last column).

From studies listed in Table 1, there is evidence that aerosols impact the EASM's precipitation intensity and distribution over China through both direct and indirect effects, but results from studies using different modeling systems (e.g., online vs. offline chemistry, prognostic vs. prescribed aerosols), model representations of physical processes, and domain configuration/spatial resolution notably vary. Online-coupled general circulation models over larger global domains at 2.8° × 2.8° horizontal resolution show that aerosol scattering and absorption impacts the atmospheric circulation and weakens the EASM during both winter and summer (Liu et al., 2009). Early regional modeling studies at 60 × 60 km showed that the aerosol microphysical effect dominated the direct radiative effect in decreasing precipitation in East Asia (Giorgi et al., 2003; Huang et al., 2007), while Zhang et al. (2012) later showed that the direct radiative forcing has an impact on surface cooling and weakening of the land/sea temperature contrast, which leads to less (more) precipitation in southern (northern) EC. Other offline-coupled chemical transport simulations demonstrated that the interactions between aerosols and the EASM are not only one-way, but rather that a decadal-scale weakening of the EASM circulation may in turn enhance aerosol concentrations through changes in convergence patterns (Zhu et al., 2012). Application of online-coupled regional climate models at a resolution of 36 × 36 km showed that during the first phase of EASM (early May – mid June), the aerosol radiative effect promotes an anticyclonic circulation in northern EC that serves to decrease precipitation in southern EC, while aerosol microphysical effects during the second EASM phase (mid-June – August) may shift the precipitation band farther north in EC (Wu et al., 2013). Implementation of a cumulus parameterization that incorporates a two-moment cloud microphysics parameterization in a coupled regional climate simulation indicates that aerosols reduce the simulated surface precipitation during the EASM by about 10% (Lim et al., 2014). This precipitation reduction was less significant when microphysical processes are excluded from the cumulus parameterization, suggesting the importance of aerosol impacts on microphysical processes of convective clouds. Use of finer spatial resolutions along with more accurate representations of the aerosol-cloud microphysical processes and their feedbacks, can provide a more accurate representation of the aerosol impacts on precipitation (e.g., Li et al., 2011). Recent regional climate simulations of the EASM, however, have only been applied to a single domain, usually at a relatively coarse 36 × 36 km horizontal resolution, while other studies do not show improvement in model performance with increased model resolution over the highly polluted regions of China (e.g., Tan et al., 2015). Hence, there is a need to perform additional investigations in the EC region using nested simulations at multiple resolutions, while evaluating the scalability of coupled models in their prediction of chemistry, aerosol, and precipitation characteristics and relationships.

The present paper uses a multiple nested (36, 12, and 4 km) and online-coupled regional climate model, and evaluates the meteorological, chemical and aerosol, cloud, and precipitation model performance during the anomalous 2010 EASM conditions over EC and the YRD region. Our main objectives are to 1) evaluate the model's performance in reproducing meteorological and chemical variables and their characteristics, 2) investigate the impacts of increased spatial resolution on the model performance that uses physics designed for a coarser resolution climate model, and 3) provide insight into the model prediction of spatiotemporal relationships between aerosol, clouds, and precipitation predictions at multiple scales during the 2010 EASM. The following sections provide the full details of our nested model, setup, and simulation design (Section 2), evaluation, observations, and model analysis methods (Section 3), results of the analysis (Section 4), and conclusions (Section 5).

2. Model setup and simulation design

2.1. Model configuration and inputs

As shown in the last column of Table 1, our work uses a variant of the Weather Research and Forecasting Model with Chemistry

Table 1
Summary of model configurations used in previous studies on aerosols and the East Asian climate, as compared to our work (last column). The references for short-names and acronyms in the table are provided in the footnote. The aerosol effects (last row) investigated in each study are Direct (D), Semidirect (S), Indirect (I), and Total (T). n.a. = not applicable.

Study	Giorgi et al. (2003)	Huang et al. (2007)	Liu et al. (2009)	Zhang et al. (2012)	Zhu et al. (2012)	Wu et al. (2013)	Lim et al. (2014)	Zhang et al. (2015)	Wang et al. (2016)	Our Work
Coupled Model System	RegCM2-GBQ02[1]	RegCM2-GBQ02[1]	CAM 3.0[2]	BCC_AGCM 2.0.1-CAM[3]	GEOS-Chem 8.02.01[4]	WRF-Chem 3.3.1[5]	WRF-Chem 3.4.1/ CAM 5.0[6]	WRF-Chem 3.5/3.5.1[6]	WRF-Chem 3.5.1[6]	WRF-Chem 3.4.1/CAM 5.1[6]
Simulation Period	Jan-93 - Dec-97	Jun-94 - Aug-95	55 years	60 years	1986–2006	May - Aug-07	Jul-08	2005, 2010	Jul 2008	Apr - Aug-10
Coupling	online	online	offline	online	offline	online	online	online	online	online
Domain(s)	East Asia	East Asia	Global	Global	Global	East Asia	East Asia	East Asia,	East Asia, North China, Beijing (one-way)	Asia, East Asia, and YRD (two-way)
Horiz. Res.	60 km	60 km	$2.8^\circ \times 2.8^\circ$	$2.8^\circ \times 2.8^\circ$	$2.0^\circ \times 2.5^\circ$	36 km	36 km	36 km	30, 10, and 3.3 km	36, 12, and 4 km
Vert. Res.	16 layers	16 layers	26 layers	26 layers	30 layers	28 layers	45 layers	23 layers	30 layers	23 layers
Gas-Phase Chem.	KQ[7]	KQ-TC[7,8]	MATCH4-Pathfinder II[9]	MOZART[10]	Full-Chemistry[4]	RADM2[11]	CBM-Z[12]	CBM-Z[12]	RADM2[11]	CBM-Z[12]
Aerosol Module	KQ[7]	KQ-TC[7,8]	MATCH4-Pathfinder II[9]	CAM[13]	Full-Chemistry[4]	MADE/ SORGAM[14]	MAM3[15]	MAM3[15]	MADE/ SORGAM[14]	MAM3[15]
Cloud Microphys.	Hsie et al. Scheme[16]	Hsie et al. Scheme [16]	RK[17]	RK − Mod[17,18]	n.a.	Lin et al. Scheme[19]	Morrison 2-moment[20]	Morrison 2-moment[20]	Lin et al. Scheme[19]	Morrison 2-moment[20]
Cumulus Paramet.	Kuo-Scheme[21]	Kuo-Scheme[21]	ZM95[22]	ZM95[22]	n.a.	GD[23]	ZM95-PB[22,24]	ZM95-PB[22,24]	GD[23]	ZM95-PB[22,24]
Aerosol Activation	QG[25]	QG[25,26]	n.a.	CAM[13]	n.a.	Ghan[27]	AR-G00[28]	AR-G00[28] and FN05[29]-K09[30]-B10[31]	AR-G00[28]	FN05[29]- K09[30]- B10[31]-BN07[32]
Aerosol Effects	D, I	D, S, I, T	D	D, S	n.a.	D, I, T	D, I	I	D, S, I	T

[1]Giorgi et al. (2002) and references therein. [2]Collins et al. (2004). [3]Wu et al. (2008); Gong et al. (2002), (2003). [4]http://acmg.seas.harvard.edu/geos/. [5]Grell et al. (2005). [6]Grell et al. (2005); Neale et al. (2010); Ma et al. (2013); Lim et al. (2014). [7]Kasibhatla et al. (1997); Qian et al. (2001). [8] Tan et al. (2002) and Chameides et al. (2002). [9]Rasch et al. (1997); Stowe et al. (1997).[10]Brasseur et al. (1998); Hauglustaine et al. (1998).[11]Stockwell et al. (1990).[12] Zaveri and Peters (1999).[13] Gong et al. (2002), (2003). [14] Ackermann et al. (1998); Schell et al. (2001).[15]Liu et al. (2012).[16] Kessler (1969); Hsie et al. (1984). [17]Rasch and Kristjansson (1998). [18] Zhang et al. (2003). [19] Lin et al. (1983); Chen and Sun (2002); Ghan et al. (1997). [20]Morrison and Gettelman (2008). [21] Anthes et al. (1987). [22] Zhang and McFarlane (1995); Zhang and Mu (2005). Song and Zhang (2011)[23] Grell and Dévényi (2002). [24] Park and Bretherton (2009). [25]Qian and Giorgi (1999). [26] Giorgi et al. (2003). [27]Ghan et al. (1997). [28]Abdul-Razzak and Ghan (2000).[29] Fountoukis and Nenes (2005), [30]Kumar et al. (2009), [31]Barahona et al. (2010), [32]Barahona and Nenes (2007).

(WRF-Chem) version 3.4.1 (Grell et al., 2005), which includes the Community Atmosphere Model (CAM) version 5.1 physical parameterizations (Neale et al., 2010) that were implemented by Ma et al. (2013), hereafter referred to as WRF-CAM5. The CAM5 physical package in this work includes an updated two-moment deep convection scheme (Zhang and McFarlane, 1995; Song and Zhang, 2011; Lim et al., 2014), the University of Washington shallow convection scheme (Park and Bretherton, 2009), a two-moment microphysics scheme (Morrison and Gettelman, 2008), a simple macrophysics scheme from CAM5 (Neale et al., 2010), and the three-mode (Aitken, Accumulation, and Coarse) modal aerosol module (MAM3) (Liu et al., 2012) coupled to the gas phase chemistry of Carbon Bond Mechanism version Z (CBMZ) (Zaveri and Peters, 1999).

Previous studies have used both offline and online-coupled modeling systems to probe the aerosol effects on climate and precipitation (Table 1); however, our work uses an online-coupled and two-way triple-nested modeling approach at high resolution that includes the Zhang and McFarlane (ZM) convective parameterization with a two-moment microphysics scheme for sub-grid cumulus clouds (Song and Zhang, 2011), as well as a two-moment scheme for grid-scale stratiform clouds (Morrison and Gettelman, 2008). As detailed in Lim et al. (2014), implementation of the new ZM scheme with two-moment cloud microphysics allows for the interactions of aerosols with microphysical processes in both resolved stratiform and parameterized cumulus clouds. Different from Lim et al. (2014), the WRF-CAM5 configuration in this work uses a more detailed aerosol activation parameterization, which is based on Fountoukis and Nenes (2005) (FN05), and includes updates from Barahona and Nenes (2007), Kumar et al. (2009), and Barahona et al. (2010). Compared to another widely used parameterization based on Abdul-Razzak and Ghan (2000) (AR-G00) that was used in Lim et al. (2014), FN05 shows better agreement of activated aerosol with a high-confidence numerical solution (Ghan et al., 2011), and with observations of shortwave radiation, cloud droplet number concentration, and precipitation (Bennartz, 2007; Zhang, 2013). Recent WRF-Chem simulations over the U.S., however, suggested that using the FN05 scheme may result in lower normalized mean bias but larger normalized mean error relative to AR-G00 for simulated CDNC against MODIS (Yahya et al., 2017).

The meteorological initial and boundary conditions (ICONs/BCONs) come from the National Centers for Environmental Prediction's Final Global Data Assimilation System (NCEP-FNL) for 2010, and the chemical ICONs/BCONs are based on chemical profiles calculated from the linked Harvard/National Aeronautics and Space Administration (NASA) Goddard Earth Observing System-Chemistry (GEOS-Chem) and U.S. EPA Community Multi-Scale Air Quality (CMAQ) model simulations from 2005 (GEOS-Chem/CMAQ). Anthropogenic emissions are based on the 2006 emission inventory for Asia in support of the Intercontinental Chemical Transport Experiment-Phase B (INTEX-B) funded by NASA (Zhang et al., 2009), and the 2010 Multi-resolution Emission Inventory for China (MEIC; http://www.meicmodel.org/). Biogenic emissions are based on MEGAN version 2 (MEGAN2; Guenther et al., 2006), dust emissions on Zender et al. (2003), and sea salt emissions on Gong et al. (2002).

2.2. Simulation design

As shown in Fig. 1, the outermost domain is centered over the continent of Asia (d01 – 36 km), and the two-way nested domains are over EC (d02 – 12 km) and YRD (d03 – 4 km). Domain d01 is comparable to many previous studies of the EASM at a grid resolution of 36 km (Table 1), and may be considered large enough to adequately cover the major parts of EC that are significantly impacted by the EASM's circulation and precipitation patterns. Simulations of aerosol impacts on clouds and precipitation are sensitive to both model resolution and choice of cumulus parameterization, and studies at cloud-resolving scales have shown that the microphysical effects are a fundamental reason for observed changes in macrophysical properties (e.g., the increases of cloud

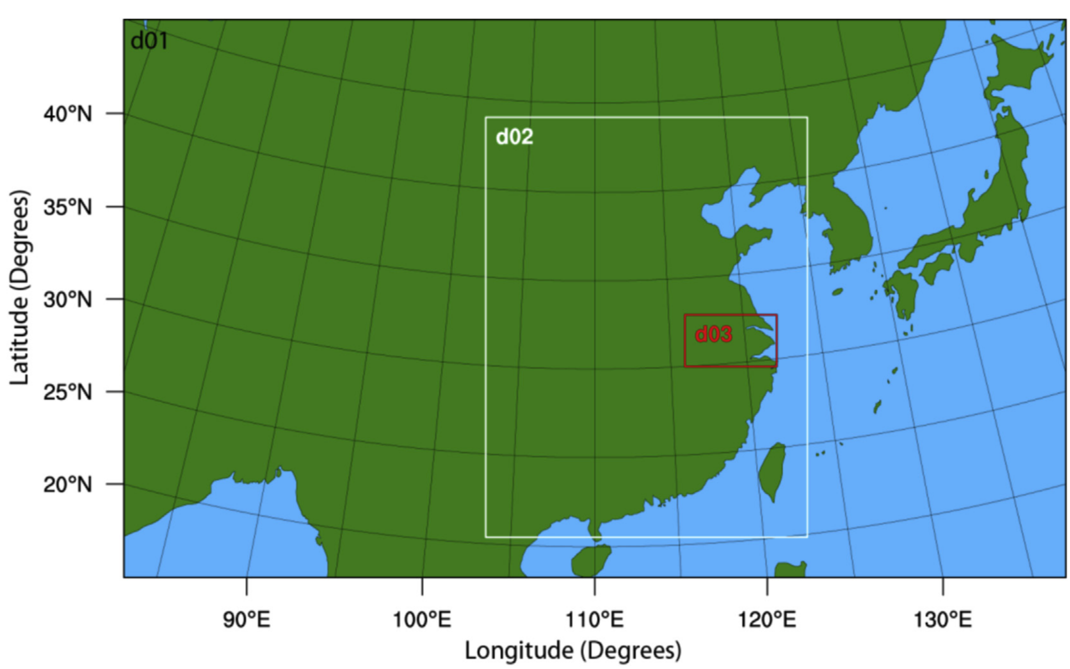

Fig. 1. Two-way nested WRF/CAM5 domain configuration for d01 (36 × 36 km) over Asia, d02 (12 × 12 km) over Eastern China, and d03 (4 × 4 km) over the Yangtze River Delta region.

cover, cloud top height, and cloud thickness) for deep convective clouds (Fan et al., 2013). In this work we use the triple-nested model domains in Fig. 1, d01, d02, and d03 to evaluate the aerosols and EASM characteristics over YRD.

While the ZM cumulus parameterization was not originally designed to run at 4 km, we chose to implement the ZM scheme for all domains, including the d03 domain at 4 km resolution, as it is well known that there is a range in cloud permitting horizontal scales, or a "gray zone", where cloud microphysics schemes have limitations in representing moist convection as the model grid spacing decreases from about 12 to 4 km (Hong and Dudhia, 2012). This gray zone is also dependent on the individual cumulus parameterization chosen, and recent efforts have been applied to develop new cumulus parameterizations that can be applied across such scales (e.g., Zheng et al., 2016). Our application of the ZM cumulus parameterization at 4 km may also be of interest to the community, as to our knowledge there has been no previous studies that apply the ZM scheme at the high resolution end ($\leq$4 km) of the gray zone. To check if the results at 4 km would be different when performing simulations with the ZM scheme and without by resolving convection, we performed a three-day test using the triple-nested configuration over d01, d02, and d03, which is the same as the configuration and design in this work, but with a test of turning off the ZM scheme (i.e., resolved convection) only for d03. We found that the differences in the daily total precipitation between the runs with ZM on and off are very small, thus indicating that using the ZM parameterization at 4 km is acceptable in this case. The results in Section 4 will provide insight into the model performance when applying ZM at increasingly higher resolutions of 36, 12, and 4 km, and the potential influence on cloud and precipitation evolution during the 2010 EASM.

The model time steps for dynamics and physics are 90, 30, and 10 s for d01, d02, and d03 respectively, and the chemistry time step was set at 300 s. The simulation time period analyzed is from May–August of 2010 (with one-month spin-up in April), which includes the onset of the EASM in the central Indochina Peninsula (April–May), through the EASM's peak advance into Northern China (July–August) (Ding, 2004).

3. Observations, evaluation protocol, and model analysis methods

3.1. Observations and model evaluation protocol

The observational data used to evaluate the model performance includes 2-m temperature (T2), 2-m water vapor mixing ratio (Q2), 10-m wind speed (WS10), and precipitation (PRECIP) from the National Climatic Data Center (NCDC; http://www.ncdc.noaa.gov). Also, a more spatially extensive comparison of model precipitation to the Tropical Rainfall Measuring Mission (TRMM) Multi-satellite Precipitation Analysis (TMPA; Huffman et al., 2007) is performed. For near-surface gas and aerosol model evaluations, a comparison against numerous air quality measurement networks include the following: 1) China's Air Pollution Index (CH-API; http://datacenter.mep.gov.cn), 2) Hong Kong (HK; http://epic.epd.gov.hk/EPICDI/air/station/?lang=en/), 3) Taiwan (TW; http://taqm.epa.gov.tw/), 4) Japan (JP; http://www.nies.go.jp/), 5) South Korea (SK; http://www.airkorea.or.kr), 6) 500 nm aerosol optical depth (AOD) measurements from NASA's Aerosol Robotic Network (AERONET; http://aeronet.gsfc.nasa.gov/), and 7) 550 nm AOD measurements from the Moderate Resolution Imaging Spectroradiometer (MODIS; Remer et al., 2005). Additional near-surface data has been retrieved from the Taihu Observatory and Xianghe sites in China, which are part of the East Asian Study of Tropospheric Aerosols: and International Regional Experiment (EAST-AIRE) data set (http://www.meto.umd.edu/~zli/EAST-AIRE/station.htm). A detailed summary describing the data frequency, uncertainty, number of sites, and their detailed sources may be found in Table A1 in Wang et al. (2017). Supplementary Section 1 provides a description of additional satellite data that are used to provide qualitative comparisons of the modeled spatial distributions for different aerosol, cloud, and precipitation characteristics.

The evaluation protocol includes statistical measures including the Mean Bias (MB), Normalized MB (NMB), Normalized Mean Error (NME), Root Mean Square Error (RMSE), Normalized RMSE (NRMSE), and Pearson's Correlation Coefficient (R). Statistical summary tables of meteorology, chemistry, cloud, and precipitation variables are included in the supplementary material. Spatial comparisons and absolute/relative difference plots are also included. The WRF-CAM5 model performance may be compared against numerous criteria that are regularly cited in the literature (e.g., Seigneur et al., 2000; U.S. EPA, 2001, 2005; Zhang et al., 2006a, 2006b; Emery et al., 2016).

3.2. Model analysis methods

The model analyses are performed over slightly modified EASM stages that are based on climatological dates of the EASM evolution across East Asia (Ding, 2004). Specifically, we compare the following: 1) The EASM Onset Stages (EOS; May–June) in continental Asia, which are characterized by the earliest onset in continental Asia that is often observed in central Indochina Peninsula in late April and early May, with areal extension and advancement eastward to the South China Sea in mid to late May, and then first arrival of the EASM into the YRD region in early June. 2) The EASM Advance Stages (EAS; June–August) in continental Asia, which are characterized by further areal advance of the EASM across the YRD region in late June, and then followed by the EASM advancing farther northward to areas of Northern China in July through August. The EOS and EAS are compared to investigate the spatial and temporal patterns of meteorological, chemical, clouds, radiation, and precipitation variables across EC and the YRD.

4. Results

4.1. Chemistry and aerosol evaluation

Fig. 2 shows a bar chart comparison of the percent NMB for simulated AOD, PM_{10}, $PM_{2.5}$, carbon monoxide (CO), nitrogen oxides ($NO_x = NO + NO_2$), ozone (O_3), and sulfur dioxide (SO_2) against surface networks across all three domains and their domain intercomparisons. The different observational networks were described in Section 3.1. Additional spatial MB plots against PM_{10} China API sites (PM10-CH-API) over d01, d02, and d03 are included in Supplementary Fig. S9.

Overall, there are predominant 1) underpredictions for AOD, surface PM_{10}, and surface $PM_{2.5}$, 2) underpredictions for surface CO, NO_x, and SO_2 concentrations, and 3) overpredictions for surface O_3 concentration. The underpredictions in AOD/PM variables are consistent with the spatial comparisons in Fig. S4a – S4f, and are likely impacted by uncertainties in primary PM emissions and secondary precursor gases, a simplified MAM3 aerosol module that does not treat PM nitrate formation, and other model treatments of processes such as wet deposition that impact aerosol concentrations. The WRF-CAM5 underpredictions in AERONET AOD, as well as qualitatively compared to MODIS observations in Figs. S4a–S4f over China, are similar to previous studies (e.g., Chen et al., 2015). The underpredictions in PM_{10} are more prominent in the northern parts of EC, while there are some overpredictions that occur in southern EC, especially near the southeast coast (Figs. S9a and S9b).

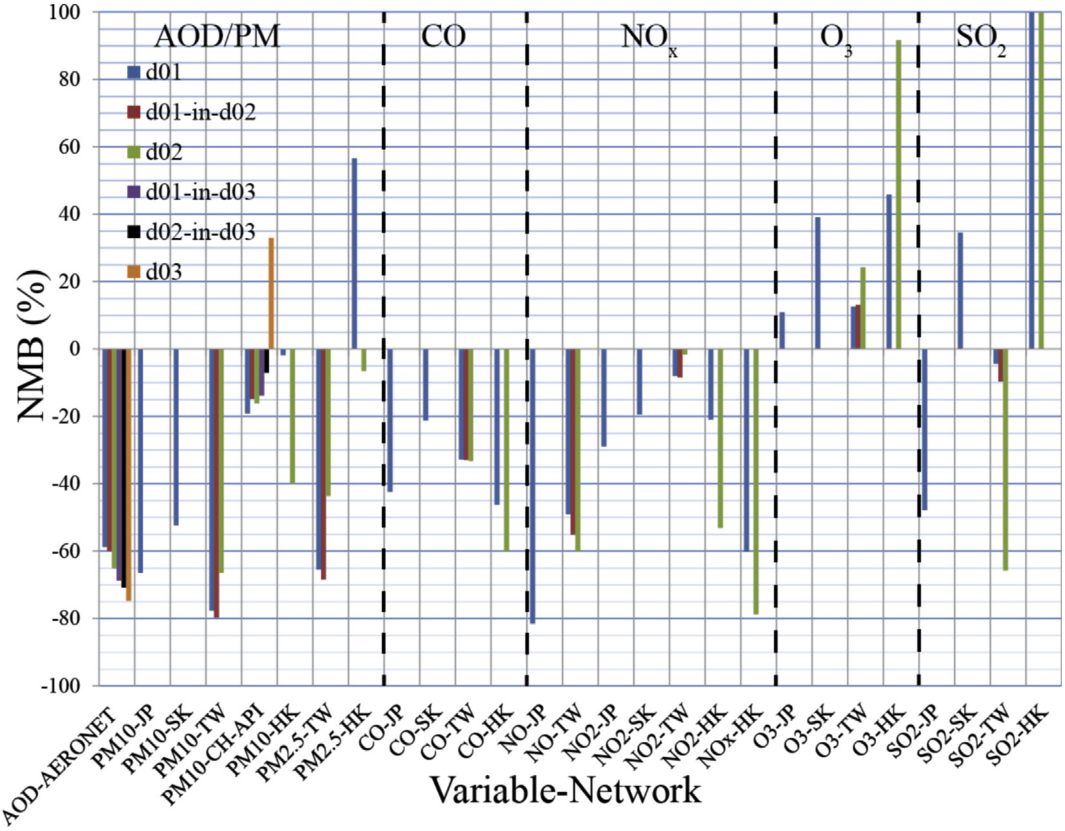

Fig. 2. Average May–August 2010 bar chart comparison of NMB for AOD, PM_{10}, $PM_{2.5}$, CO, NO, NO_2, NO_x, TOR, O_3, and SO_2 over d01 (blue; 36 km), d01-in-d02 (red; 36 km), d02 (green; 12 km), d01-in-d03 (purple; 36 km), d02-in-d03 (black; 12 km), and d03 (orange; 4 km) domains. The x-axis includes the short name for each variable and network, as described in the text. The full statistics are provided in Table S1. (For interpretation of the references to colour in this figure legend, the reader is referred to the web version of this article.)

There is evidence that the surface PM underpredictions have a strong impact on the column AOD underpredictions. The NMBs against MODIS and AERONET AOD are within 10% of one another (Table S1), and the NMB magnitude increases as spatial resolution is increased. There are however decreases in NMB when increasing model resolution from 36 (d01-in-d02 and d01-in-d03) to 12 km (d02 and d02-in-d03) for surface PM_{10} and $PM_{2.5}$ at the China-API (PM10-CH-API and PM2.5-CH-API) and Taiwan (PM2.5-TW) sites. The disparity in sensitivity of model performance to increasing model resolution for the column and surface PM indicates that increasing resolution can lead to an improvement in the representation of local emissions and vertical distribution impacts on surface PM concentrations, while at the same time degrading the model performance of column PM due to impacts from other dynamic and meteorological processes (e.g., precipitation and wet deposition) that are also changed by increasing model resolution. The number of relatively large overpredictions over a few sites in the YRD (See Fig. S9c) leads to a domain wide average positive NMB for PM10-CH-API in d03 (Fig. 2). The anomalous positive NMB for $PM_{2.5}$ over Hong Kong (PM2.5-HK) for d01 is driven by a large overprediction in precursor SO_2 concentration in d01 (Fig. 2; SO2-HK ~ 244%), which is likely due to emission uncertainties in the MEIC. In spite of the large overprediction in SO_2 concentration for d02 (Fig. 2; SO2-HK ~ 147%), the small underprediction in PM2.5-HK is due to an overprediction of precipitation for d02 compared to d01 (approximate comparison in Fig. S1), thus inferring more wet deposition of $PM_{2.5}$.

For the gas concentrations of CO and NO_x there are consistent underpredictions; however, there are approximate overpredictions against domain-wide average column observations of CO and NO_x at all resolutions. There are both under and overpredictions for surface SO_2 depending on the specific observational network. Fig. S10 shows approximate spatial comparisons of observed and simulated column CO, NO_x, and SO_2 over d01, d02, and d03. Overall there is a good agreement in the spatial distribution of column CO, NO_2, and SO_2, and the statistics are generally better for the column abundances compared to the near-surface observations, with notably higher R correlation coefficients (Table S1).

Fig. 3 presents a time series comparison for 500 nm AOD at eight AERONET sites and the representative simulated values from the closest model grid point, shown in order of the highest to lowest mean observed AOD values for each site.

There are typically higher AOD values during the May–June (~EOS) period compared to the July–August period of the EASM (~EAS) for 7 out of the 8 AERONET sites. The model generally captures the decreasing trend in AOD from May–August 2010 during the EOS and EAS; however, the model consistently underpredicts AOD for d01, d02, and d03 at most of the sites (Fig. 3a–f), except at the Minqin and Lulin sites (Fig. 3g–h), where there is closer agreement with relatively lower AOD values compared to the other sites.

4.2. Precipitation evaluation

Fig. 4 shows the May–August 2010 cumulative probability distribution functions (CDF) of model convective, grid-resolved, and total rain compared against the TMPA observed total rain for all rain periods (>0 mm day^{-1}), heavy rain periods (>25 mm day^{-1}), and

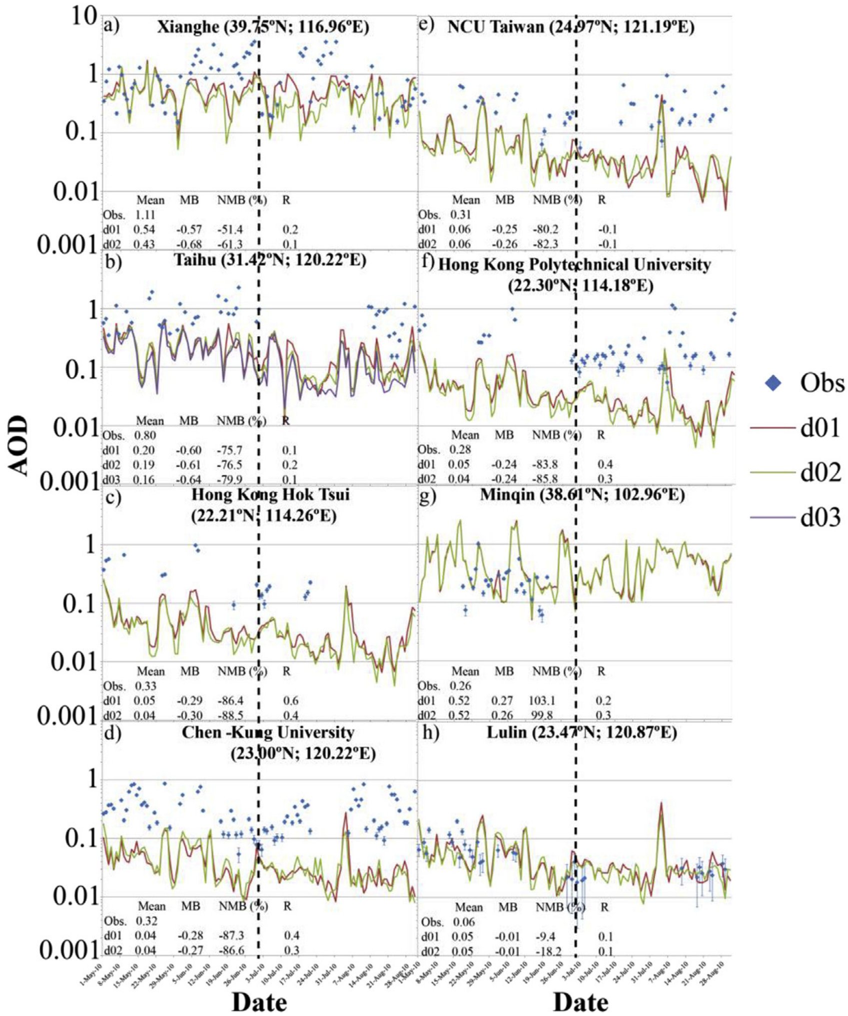

Fig. 3. May–August 2010 time series plots for observed AERONET AOD at 500 nm (blue symbols) at a) Xianghe, b) Taihu, c) Hong Kong Hok Tsui, d) Chen-Kung University, e) NCU Taiwan, f) Hong Kong Polytechnical University, g) Minqin, and h) Lulin sites, compared against simulated AOD at 500 nm for d01 (red), d02 (green), and d03 (purple; Taihu only). The mean, MB, NMB, and correlation statistics are presented in the lower left corner of each panel. Vertical dashed line approximately separates the EOS from EAS time periods. The full statistics are provided in Table S1. (For interpretation of the references to colour in this figure legend, the reader is referred to the web version of this article.)

light rain periods (<10 mm day^{-1}).

There is relatively low average NMB for rain across EC (d02) and YRD (d03) for different model resolutions (Supplementary Figs. S1–S2 and Table S1); however, the CDF comparisons show some notable differences. When considering all rain periods in EC and YRD, the model grid-resolved and total rain have a similar CDF, and they are both quite different compared to the observed total rain CDF, which is more similar to the model convective rain CDF (Fig. 4a and b). This suggests that the predominant contribution to the model total rain distribution is from the grid-resolved rain, but that their distributions do not as accurately represent the observed total rain distribution, which is more closely resembled by the convective rain distribution across EC and YRD. There is a similar result when considering only the heavy rain periods (Fig. 4c and d), where the observed total rain distribution falls in the middle of the model grid-resolved, convective, and total rain in EC, but the model convective CDF is very similar to the observed total rain CDF in YRD. For the light rain periods only (Fig. 4e and f), the model convective CDF is very close to the observed total rain CDF, especially over EC where they are nearly identical. The model total and grid-resolved rain CDFs are progressively farther from the observed rain distribution, again demonstrating the limitation of the WRF-CAM5 model physics to accurately depict the partitioning between grid-resolved and convective rain that each contribute to the total rain during light rain periods, while also suggesting the importance of the convective-type rain distributions during these periods and for these scales. A direct comparison of the model and observed total rain CDFs during all periods in Fig. 4, shows that the predicted distribution is too steep, especially at the lower rain rates, which further suggests an overall larger frequency of underpredicted rain compared to the observations across the EC and YRD domains.

4.3. Aerosol, cloud, and precipitation comparisons

Fig. 5 shows a time series-meridional structure (i.e., zonal average) analysis of model column AOD, CCN, CDNC, COT, and surface PRECIP compared to observed TMPA precipitation for the d01-in-d02, d02, d02-in-d03, and d03 domains. Supplementary Fig. S11 also provides a similar analysis for near-surface dust, PM_{10}, $PM_{2.5}$, SO_4^{2-}, BC, OA, and SOA concentrations.

For d01-in-d02 and d02 over EC, the AOD is the highest at the beginning of the EOS in early to mid-May, it decreases to lower values by the start of the EAS in early July, and higher values resume towards the end of the EAS (Fig. 5a and b). The spatiotemporal

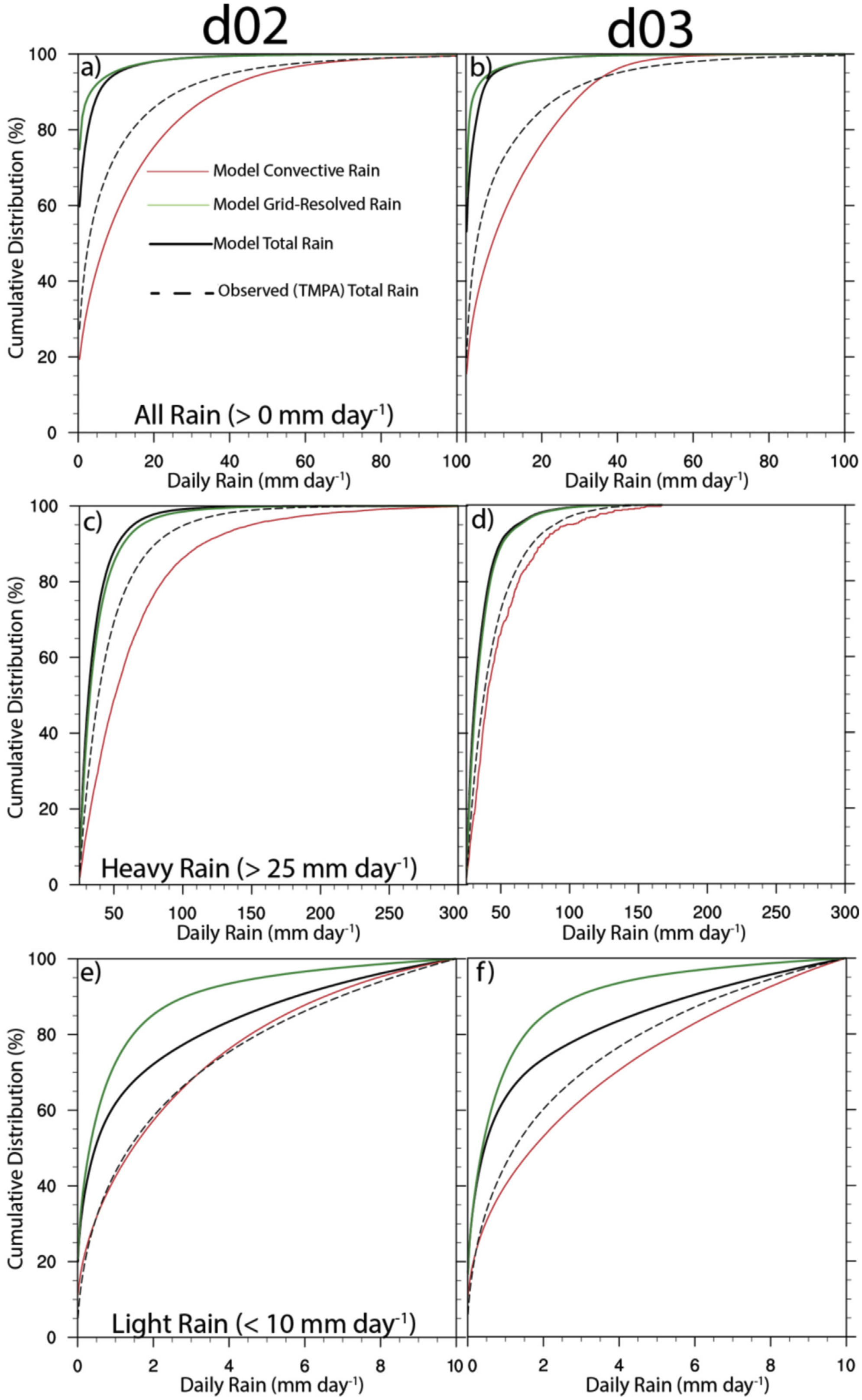

Fig. 4. Cumulative probability distribution function (CDF) plots of model convective (red), model grid-scale (green), model total (solid black), and TMPA observed total (dashed black) daily rain (mm day^{-1}) in EC (d02; left) and YRD (d03; right) for a) – b) all rain periods, c) – d) heavy rain periods only, and e) – f) light rain periods only. (For interpretation of the references to colour in this figure legend, the reader is referred to the web version of this article.)

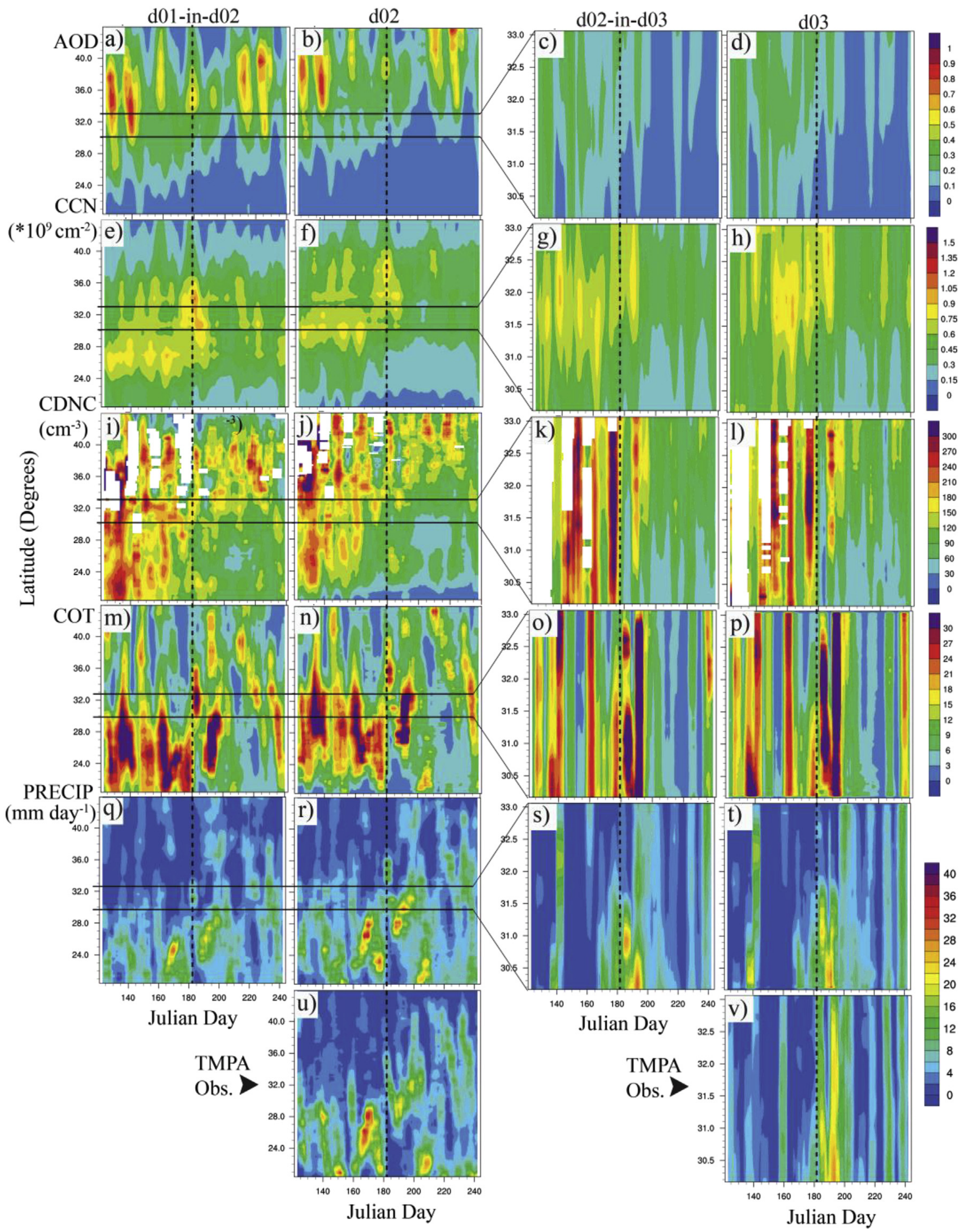

Fig. 5. Time-series meridional structure analysis over d01-in-d02 (first column), d02 (second column), d02-in-d03 (third column), and d03 (fourth column) for simulated a) – d) column AOD, e) – h) column CCN at 0.5% supersaturation, i) – l) column CDNC, m) – p) column COT, q) – t) surface PRECIP, and u) – v) observed TMPA PRECIP. Values are 5-day running averages. Time period on the x-axis pertains to Julian Day 121–243 (May 01 – August 31, 2010). Vertical dashed line generally separates the EOS from EAS time periods.

pattern of the enhanced AOD band qualitatively agrees with enhanced bands of surface dust, PM_{10}, and $PM_{2.5}$, indicating a strong impact of surface PM on the column abundance in d01-in-d02 and d02 (Figs. S11a, S11b, S11e, S11f, S11i, and S11j). The clear northward shift in the enhanced aerosol band from the EOS to EAS is largely influenced by the northward shift of the enhanced SO_4^{2-} concentrations (Fig. S11m and S11n), and the AOD and PM concentrations are less in the EAS compared to the EOS. In EC, cloud and precipitation (Fig. 5q and r) are generally influenced by the northward propagation of the Meiyu front during the summer monsoon season. Since wet deposition is an important mechanism for aerosol removal, the spatiotemporal distributions of AOD and

PRECIP are also distinctly complementary. Generally, AOD in d02 is displaced further north compared to d01-in-d02, consistent with the more northward rain band in d02 compared to d01-in-d02.

The AODs in d02-in-d03 and d03 over the YRD region are largely comparable; both showing higher values during the early EOS across all latitudes, and then decreases through the EAS (Fig. 5c and d). Over YRD, dust concentrations are very low during both EOS and EAS (Figs. S8c and S8d), but the spatial patterns of surface PM_{10} and $PM_{2.5}$ are comparable to that of the column AOD, which suggests that anthropogenic PM sources dominate over the natural sources in the YRD during EASM. In fact, SO_4^{2-} and OA have relatively larger fractional contributions to the $PM_{2.5}$ load over EC in d02, while SO_4^{2-}, OA, and SOA have high contributions to $PM_{2.5}$ over YRD in d03 (Figures not shown).

Although high CCN values also display a general northward shift over time, the peak CCN values are farther south compared to the peak AOD values in d01-in-d02 and d02 (Fig. 5e–f). This suggests that the model may not account for the larger size dust particles (Fig. S11a – S11b) because the aerosol size distribution and hygroscopicity assumptions in the model may limit the maximum size of the dust particles to act as giant CCN at 0.5% supersaturation. The smaller SO_4^{2-} particles (Fig. S11m – S11n) have better spatiotemporal agreement with the CCN patterns over EC in d02. This is partly related to the lower moisture in the north during the EOS. Over YRD in d03, there is good agreement between the enhanced column CCN and AOD during the EOS, along with similar patterns in surface $PM_{2.5}$, SO_4^{2-}, BC, OA, and SOA (Fig. S11).

In regards to the spatiotemporal patterns of cloud variables, the CDNC is the highest during the EOS, with relatively large values extending across all latitudes over EC in d01-in-d02 and d02 (Fig. 5i and j). The CDNC decreases and moves northward during EAS, with the most elevated CDNC values north of about 33°N. This spatiotemporal pattern of enhanced CDNC qualitatively agrees well with the AOD, while CDNC shows less agreement with CCN at 0.5% supersaturation, as this CCN supersaturation estimation is likely smaller than many of the in-cloud supersaturation points. Similar relationships of AOD, CCN, and CDNC exist over YRD in d02-in-d03 and d03 (Fig. 5k and l), and the CDNC decreases during the EOS to EAS transition likely due to less clouds forming. The COT over EC is also most enhanced during EOS, and then decreases and shifts slightly north during EAS, where the most enhanced COT values are mainly found south of 33°N (Fig. 5m and n), which coincides with the higher water vapor concentrations and higher PRECIP (Figs. S2c and S2g). Similar spatiotemporal distributions of CDNC, COT, and PRECIP as well as their relationships are also found in YRD. The PRECIP in d02 has a better agreement with the observed TMPA PRECIP (Fig. 5u) than d01-in-d02. Similarly, the simulated precipitation over d03 is in better agreement with the TMPA observed precipitation (Fig. 5v) than d02-in-d03. These comparisons further establish that WRF-CAM5 can exhibit improved skill in simulating precipitation with increasing model resolution in EC and YRD, and the basic applicability of using the ZM cumulus parameterization down to at least 4 km horizontal resolution.

To further investigate the interconnections between the simulated aerosol, cloud, convection, and precipitation predictions during the 2010 EASM, we identify 5-day periods when the model largely overpredicts an observed light precipitation period (O_LPP), and also largely underpredicts an observed heavy precipitation period (U_HPP) across the YRD domain d03. Fig. 6 shows an average d03 time series of NCDC and TMPA observed precipitation compared against the modeled precipitation (Fig. 6a), and the contributions of modeled convective and grid-resolved precipitation to the total (Fig. 6b).

Overall the model qualitatively does a good job in the timing of the NCDC and TMPA daily precipitation patterns; however, in many instances the simulated magnitude is either underpredicted or overpredicted (Fig. 6a). On May 20–24 during EOS, the model largely overpredicts the precipitation observed by both NCDC and TMPA (i.e., O_LPP), and just after the start of EAS on July 09–13, the model largely underpredicts a relatively heavy precipitation period that was observed (i.e., U_HPP). In both of these cases, the modeled O_LPP and U_HPP total precipitation is dominated by grid-scale precipitation predictions; however, there is a larger contribution from the convective precipitation for the U_HPP compared to the O_LPP (Fig. 6b).

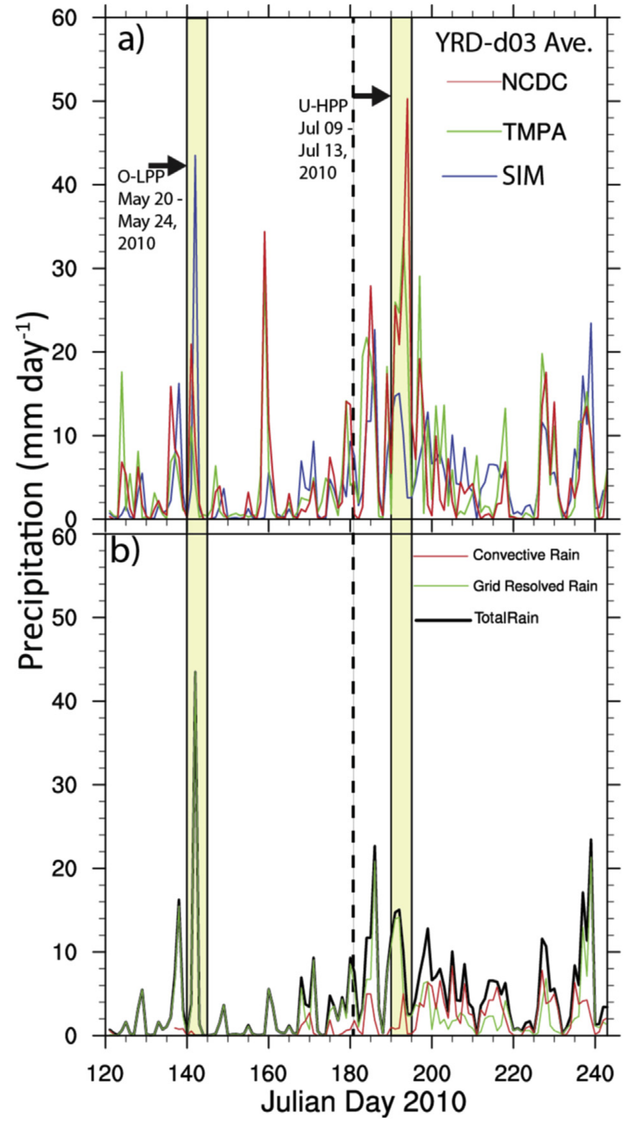

Fig. 6. 2010 time series of a) observed NCDC (red), observed TMPA (green), and simulated daily precipitation (blue), and b) simulated convective (red), grid-scale (green), and total daily precipitation (black) averaged over domain d03 (YRD; 4 km). The yellow shaded areas represent the overpredicted light precipitation period (O-LPP) and the underpredicted heavy precipitation period (U-HPP). The vertical dashed line generally separates the EOS from EAS time periods. (For interpretation of the references to colour in this figure legend, the reader is referred to the web version of this article.)

Fig. 7 shows spatial comparisons of observed TMPA and modeled total precipitation averaged over the O-LPP and U-HPP periods in YRD, as well as each period's near-surface aerosol number concentration, total PM_{10} mass concentration, and CCN number at a supersaturation of 0.5%.

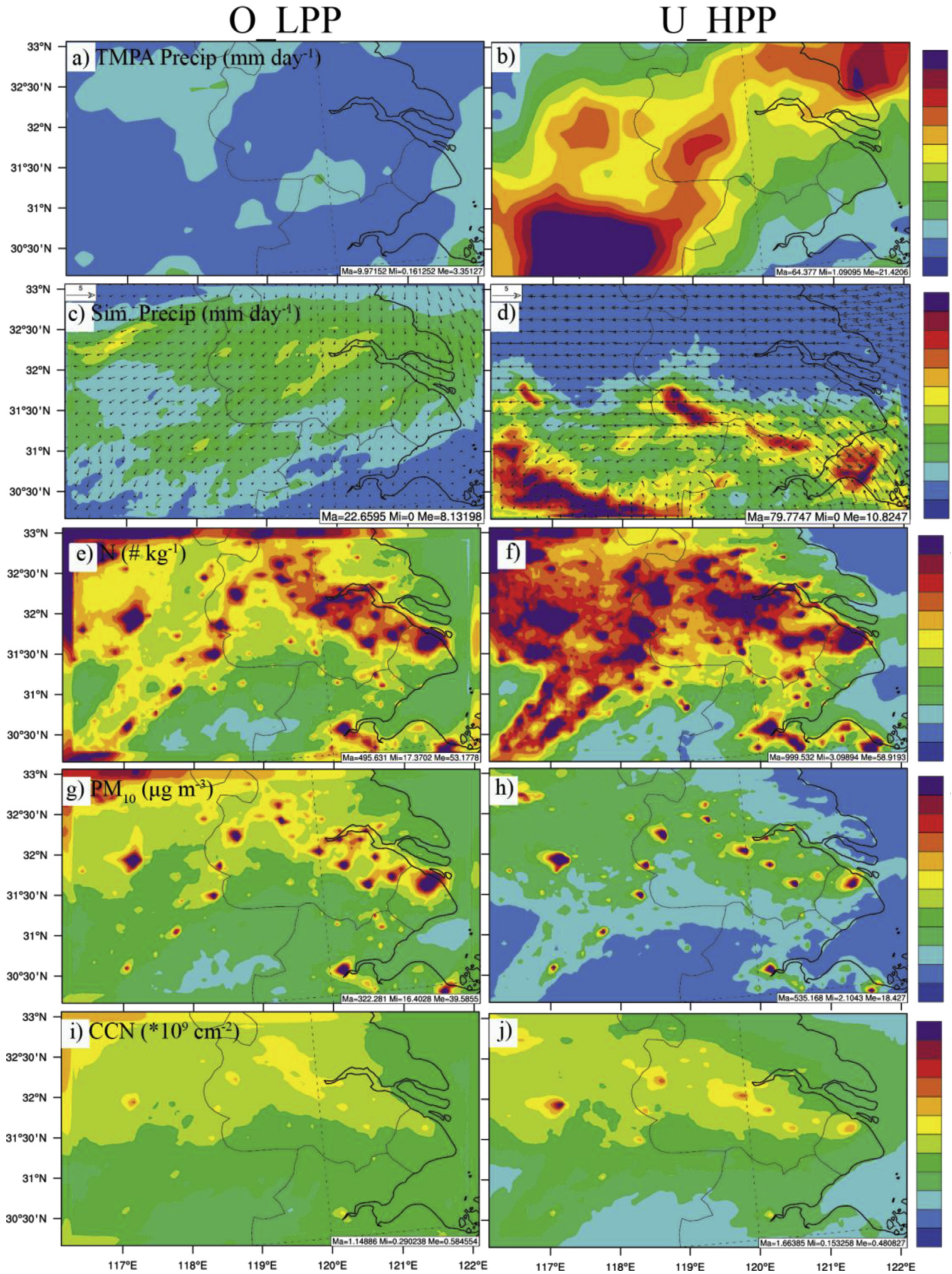

Fig. 7. Average 5-day O_LPP and U_HPP spatial plots of a) – b) observed TMPA precipitation and c) – d) simulated precipitation, e) – f) simulated total aerosol number, g) – h) simulated mass concentration of PM_{10}, and i) – j) simulated CCN number for domain d03.

The O_LPP and U_HPP are both maximized north of about 32°N (Fig. 7a–d), where the O_LPP has relatively lower total aerosol number concentrations (Fig. 7e–f), but larger total PM_{10} mass concentrations (Fig. 7g–h) compared to the U_HPP. There is limited observational aerosol and cloud data over YRD for comparison during these periods; however, these results suggest that the U_HPP has a larger number of aerosol available for CCN compared to O_LPP (Fig. 7i–j), which in conjunction with a similar water vapor available for condensation may lead to a larger abundance of small CDNC that generate less precipitation for U_HPP compared to O_LPP. Such a large underestimation of the heavy precipitation, however, may also be because the model did not accurately simulate the overall convective system, which is largely controlled by the convective available potential energy (CAPE). While it was only analyzed for the average May–August 2010 period, Fig. S7 shows large areas of underpredicted T2 over YRD, which would corroborate an underprediction in the overall convective system during U_HPP. Thus the aerosol impacts on convective intensity shown here can only be assumed to be a secondary effect to an underprediction in CAPE. Nonetheless, there is some evidence that the WRF-CAM5 aerosol predictability impacts the predictability of light and heavy precipitation events over YRD during the 2010 EASM. These results help place into context previous studies that used WRF-CAM5 and MAM3 aerosol simulations for similar regions and time periods, and suggests the need for continuous implementation of more developed aerosol and cloud model components/interactions for application to regional scale studies.

5. Summary and conclusions

An online-coupled WRF-CAM5 simulation for the months of May–August 2010 was implemented to evaluate its meteorological and chemical performance, assess the model predictions of spatial and temporal aerosol characteristics, and ultimately how such model physics designed for a coarser resolution climate model (i.e., CAM5) impacts precipitation performance during the East Asian Summer Monsoon (EASM) at the continental (d01 − 36 km; over Asia), regional (d02 − 12 km; over Eastern China; EC), and near-cloud resolving scales (d03 − 4 km; over Yangtze River Delta; YRD). The WRF-CAM5 model performs well for meteorological variables T2, Q2, and WS10 against NCDC with NMBs within ±5% and NRMSE values < 0.5 across all domains. The model does not perform well for many cloud and radiation variables, and there are apparent underpredictions for cloud condensation nuclei (CCN), cloud optical thickness (COT), and liquid (LWP) and ice water path (IWP) determined by qualitative comparisons against satellite estimations. The model performs better for precipitation, and thus suggests that cloud and radiation predictions and evaluation methods need to be improved here, especially for cloud microphysical and macrophysical variables that are very important to the development of rain. Cumulative probability distribution functions of precipitation show that there is a larger frequency of underpredicted total rain compared to the observations across the EC and YRD domains, while suggesting the importance of the contribution of a convective rain distribution to the total rain, and a model deficiency in accurately predicting convective rain in this WRF-CAM5 configuration. The model performance also demonstrates a dependence on model grid resolution in some cases.

The AOD is most enhanced over northwestern and northern China, as well as over the YRD region. Although there is good spatial agreement, WRF-CAM5 underpredicts the magnitude of AOD, and has an average NMB of about −55%, −62%, and −81% against MODIS AOD, and about −59%, −65%, and −75% against AERONET AOD for d01, d02, and d03 respectively. There is a clear relationship between enhanced AOD values and surface PM_{10} and $PM_{2.5}$, with significant contributions from anthropogenic SO_4^{2-}, BC, and organic PM to the localized $PM_{2.5}$ maxima over EC and YRD. There are model underpredictions for PM_{10} and $PM_{2.5}$, in part due to underpredictions in emissions of primary PM and precursor gases such as SO_2. The model NMB increases for AOD with increasing spatial resolution, while there is reduced NMB against surface PM_{10} and $PM_{2.5}$ when increasing model resolution. Increasing model resolution may lead to a better representation of local emissions and vertical distribution on surface concentration, while at the same time worsening the accuracy of the parameterization of other dynamic and meteorological processes at finer resolution that impact column AOD. The model generally captures the trend in decreasing AOD values during the May–June (EOS) period compared to the July–August (EAS) period, but consistently underpredicts AOD for d01, d02, and d03 at sites with relatively higher AOD.

The surface PM and column AOD are most enhanced between about 32°N and 42°N in early to mid-May during the EOS, and then shifts north during the EAS in July and August. The northward shift is evident in the SO_4^{2-} concentrations as well. Over both EC and YRD, the AOD and PM are higher during the EOS compared to the EAS, and there are relatively larger anthropogenic sources of PM compared to natural sources during both periods. The spatiotemporal trends of AOD and CDNC agree during the EOS to EAS transition over EC. There is also lower CDNC and higher COT near regions of lower AOD during EOS and EAS, especially south of 33°N due to relatively higher water vapor abundance and lower aerosol concentrations in this region. Increasing spatial resolution from 36 km to 12 km over the EC region shows somewhat different patterns for the spatiotemporal evolution of aerosols and their composition, related cloud variables, and precipitation, and the simulation over d02 had better agreement with the observed TMPA PRECIP compared to d01-in-d02. Over the YRD region, there is relatively enhanced AOD and CDNC and lower COT during the EOS compared to EAS. The simulated precipitation over d03 has better agreement with TMPA observations compared to d02-in-d03.

These results demonstrate the overall adequacy of WRF-CAM5 in predicting the characteristics and evolution of aerosols and precipitation during relatively large-scale dynamic changes (e.g., EASM) at regional scales from 36 to 4 km At the same time, however, the results present significant underpredictions in aerosols, as well as large over (O_LPP) and underpredictions (U_HPP) in precipitation events, which highlight existing weaknesses when applying WRF-CAM5 physics to regional and local-scale investigations. There are inherently some limitations in modeling the aerosol, cloud, and precipitation interactions accurately with a relatively older WRF-Chem version 3.4.1 in WRF-CAM5, especially when compared to the most recent version of WRF-Chem that has undergone substantial improvement by the time of writing this paper (i.e., version 3.9.1). In a recent comprehensive evaluation of WRF-CAM5 (also with WRF-Chem version 3.4.1) by He et al. (2017), they also demonstrate that this model can generally reproduce meteorology, chemistry, and climate well, but that that the uncertainties in aerosol and cloud treatments contribute the most to the model biases. Thus the results of He et al. (2017) further corroborate the overall conclusions in the present paper, while further emphasizing the need to reduce such biases for future investigations of aerosol-cloud interactions.

Acknowledgements

This work was sponsored by U.S. Department of Energy, Office of Science Biological and Environmental Research as part of the Regional and Global Climate Modeling program (DE-SC0006695) and China National Basic Research Program (2010CB951803). This work used the Extreme Science and Engineering Discovery

Environment (XSEDE) (STAMPEDE), which is supported by National Science Foundation grant number OCI-1053575. The Pacific Northwest National Laboratory is operated for DOE by Battelle Memorial Institute under contract DE-AC05-76RL01830.

Appendix A. Supplementary data

Supplementary data related to this article can be found at http://dx.doi.org/10.1016/j.atmosenv.2017.09.008.

References

Abdul-Razzak, H., Ghan, S.J., 2000. A parameterization of aerosol activation: 2. Multiple aerosol types. J. Geophys. Res. 105 (D5), 6837–6844. http://dx.doi.org/10.1029/1999JD901161.

Ackermann, I.J., Hass, H., Memmesheimer, M., Ebel, A., Binkowski, F.S., Shankar, U., 1998. Modal aerosol dynamics model for Europe: development and first applications. Atmos. Environ. 32 (17), 2981–2999. http://dx.doi.org/10.1016/S1352-2310(98)00006-5.

Anthes, R.A., Hsie, E.Y., Kuo, Y.H., 1987. Description of the Penn State/NCAR Mesoscale Model Version 4 (MM4). Tech. Note NCAR/TN-282+STR, Natl. Cent. for Atmos. Res., Boulder, Colo.

Barahona, D., Nenes, A., 2007. Parameterization of cloud droplet formation in large-scale models: including effects of entrainment. J. Geophys. Res. 112, D16206. http://dx.doi.org/10.1029/2007JD008473.

Barahona, D., West, R.E.L., Stier, P., Romakkaniemi, S., Kokkola, H., Nenes, A., 2010. Comprehensively accounting for the effect of giant CCN in cloud activation parameterizations. Atmos. Chem. Phys. 10, 2467–2473. http://dx.doi.org/10.5194/acp-10-2467-2010.

Bennartz, R., 2007. Global assessment of marine boundary layer cloud droplet number concentration from satellite. J. Geophys. Res. 112, D02201. http://dx.doi.org/10.1029/2006JD007547.

Brasseur, G.P., Hauglustaine, D.A., Walters, S., Rasch, P.J., Muller, J.F., Granier, C., Tie, X.X., 1998. MOZART, a global chemical transport model for ozone and related chemical tracers 1. Model description. J. Geophys Res. 103, 28265–28289. http://dx.doi.org/10.1029/98JD02397.

Chameides, W.L., Luo, C., Saylor, R., Streets, D., Huang, Y., Bergin, M., Giorgi, F., 2002. Correlation between model-calculated anthropogenic aerosols and satellite-derived cloud optical depths: indication of indirect effect? J. Geophys. Res. 107 (D10), 4085,. http://dx.doi.org/10.1029/2000JD000208.

Chen, S.-H., Sun, W.-Y., 2002. A one-dimensional time dependent cloud model. J. Meteorol. Soc. Jpn. 80, 99–118. http://dx.doi.org/10.2151/jmsj.80.99.

Chen, Y., Zhang, Y., Fan, J., Leung, R.L.-Y., Zhang, Q., He, K., 2015. Application of an online-coupled regional climate model, WRF-CAM5, over East Asia for examination of ice nucleation schemes: Part I. Comprehensive model evaluation and trend analysis for 2006 and 2011. Climate 3, 627–667. http://dx.doi.org/10.3390/cli3030627.

Cheng, Z., Wanga, S., Jianga, J., Fuc, Q., Chend, C., Xue, B., Yuf, J., Fua, X., Hao, J., 2013. Long-term trend of haze pollution and impact of particulate matter in the Yangtze River Delta, China. Environ. Pollut. 182, 101–110. http://dx.doi.org/10.1016/j.envpol.2013.06.043.

Collins, W.D., Rasch, P.J., Boville, B.A., Hack, J.J., McCaa, J.R., co-authors, 2004. Description of the NCAR Community Atmosphere Model (CAM3.0). NCAR Tech. Note, NCAR TN-464+STR, xii+214 pp.

Ding, A.J., Fu, C.B., Yang, X.Q., Sun, J.N., Zheng, L.F., Xie, Y.N., Herrmann, E., Nie, W., Petäjä, T., Kerminen, V.-M., Kulmala, M., 2013. Ozone and fine particle in the western Yangtze River Delta: an overview of 1 yr data at the SORPES station. Atmos. Chem. Phys. 13, 5813–5830. http://dx.doi.org/10.5194/acp-13-5813-2013.

Ding, Y.H., 2004. Seasonal march of the East Asian summer monsoon. In: Chang, C.P. (Ed.), The East Asian Monsoon. World Scientific Publisher, Singapore, 560 pp.

Emery, C., Tai, E., Yarwood, G., 2016. Enhanced Meteorological Modeling and Performance Evaluation for Two Texas Ozone Episodes. Final Report, The Texas Natural Resource Conservation Commission, 12118 Park 35 Circle Austin, Texas 78753. Available online: http://www.tceq.state.tx.us/assets/public/implementation/air/am/contracts/reports/mm/EnhancedMetModelingAndPerformanceEvaluation.pdf. (Accessed 5 May 2016).

Fan, J., Leung, L.R., Rosenfeld, D., Chen, Q., Li, Z., Zhang, J., Yan, H., 2013. Microphysical effects determine macrophysical response for aerosol impacts on deep convective clouds. PNAS 110 (48), E4581–E4590. http://dx.doi.org/10.1073/pnas.1316830110.

Fountoukis, C., Nenes, A., 2005. Continued development of a cloud droplet formation parameterization for global climate models. J. Geophys. Res. 110, D11212. http://dx.doi.org/10.1029/2004JD005591.

Ghan, S.J., Leung, L.R., Easter, R.C., Abdul-Razzak, H., 1997. Prediction of cloud droplet number in a general circulation model. J. Geophys. Res. 102 (D18), 21,777–21,794. http://dx.doi.org/10.1029/97JD01810.

Ghan, S.J., Abdul-Razzak, H., Nenes, A., Ming, Y., Liu, X., Ovchinnikov, M., Shipway, B., Mekhidze, N., Xu, J., Shi, X., 2011. Droplet nucleation: physically-based parameterizations and comparative evaluation. J. Adv. Model. Earth Syst. 3, M10001. http://dx.doi.org/10.1029/2011MS000074.

Giorgi, F., Bi, X., Qian, Y., 2002. Direct radiative forcing and regional climatic effects of anthropogenic aerosols over East Asia: a regional coupled climate-chemistry/aerosol model study. J. Geophys. Res. 107 (D20), 4439. http://dx.doi.org/10.1029/2001JD001066.

Giorgi, F., Bi, X.Q., Qian, Y., 2003. Indirect vs. direct effects of anthropogenic sulfate on the climate of east Asia as simulated with a regional coupled climate-chemistry/aerosol model. Clim. Change 58, 345–376. http://dx.doi.org/10.1023/A:1023946010350.

Gong, S.L., Barrie, L.A., Lazare, M., 2002. Canadian aerosol module: a size-segregated simulation of atmospheric aerosol processes for climate and air quality models 2. Global sea-salt aerosol and its budgets. J. Geophys. Res. 107 http://dx.doi.org/10.1029/2001JD002004.

Gong, S.L., Barrie, L.A., Blanchet, J.-P., von Salzen, K., Lohmann, U., Lesins, G., Spacek, L., Zhang, L.M., Girard, E., Lin, H., Leaitch, R., Leighton, H., Chylek, P., Huang, P., 2003. Canadian aerosol module: a size-segregated simulation of atmospheric aerosol processes for climate and air quality models 1. Module development. J. Geophys Res. 108 http://dx.doi.org/10.1029/2001JD002002.

Grell, G.A., Dévényi, D., 2002. A generalized approach to parameterizing convection combining ensemble and data assimilation techniques. Geophys. Res. Lett. 29 (14), 1693,. http://dx.doi.org/10.1029/2002GL015311.

Grell, G.A., Peckham, S.E., Schmitz, R., McKeen, S.A., Frost, G., Skamarock, W.C., Eder, B., 2005. Fully coupled "online" chemistry within the WRF model. Atmos. Environ. 39, 6957–6975. http://dx.doi.org/10.1016/j.atmosenv.2005.04.027.

Guenther, A., Karl, T., Harley, P., Wiedinmyer, C., Palmer, P.I., Geron, C., 2006. Estimates of global terrestrial isoprene emissions using MEGAN (model of emissions of gases and aerosols from nature). Atmos. Chem. Phys. 6, 3181–3210. http://dx.doi.org/10.5194/acp-6-3181-2006.

Hauglustaine, D.A., Brasseur, G.P., Walters, S., Rasch, P.J., Muller, J.-F., Emmons, L.K., Carroll, M.A., 1998. MOZART, a global chemical transport model for ozone and related chemical tracers 2. Model results and evaluation. J. Geophys Res. 103, 28291–28335. http://dx.doi.org/10.1029/98JD02398.

He, J., Zhang, Y., Wang, K., Chen, Y., Leung, L.R., Fan, J., Li, M., Zheng, B., Zhang, Q., Duan, F., He, K., 2017. Multi-year application of WRF-CAM5 over East Asia-Part I: comprehensive evaluation and formation regimes of O3 and PM2.5. Atmos. Environ. 165, 122–142. http://dx.doi.org/10.1016/j.atmosenv.2017.06.015.

Hong, S.-Y., Dudhia, J., 2012. Next-generation Numerical Weather Prediction: Bridging Parameterization, Explicit Clouds, and Large Eddies. BAMS. http://dx.doi.org/10.1175/2011BAMS3224.1.

Hsie, E.Y., Anthes, R.A., Keyer, D., 1984. Numerical simulation of frontogenesis in a moist atmosphere. J. Atmos. Sci. 41, 2581–2594. http://dx.doi.org/10.1175/1520-0469(1984)041<2581:NSOFIA>2.0.CO;2.

Huang, Y., Chameides, W.L., Dickinson, R.E., 2007. Direct and indirect effects of anthropogenic aerosols on regional precipitation over East Asia. J. Geophys. Res. 112, D03212. http://dx.doi.org/10.1029/2006JD007114.

Huffman, G., Bolvin, J.,D.T., Nelkin, E.J., Wolff, D.B., Adler, R.F., Gu, G., Hong, Y., Bowman, K.P., Stocker, E.F., 2007. The TRMM multisatellite precipitation analysis (TMPA): quasi-global, multiyear, combined-sensor precipitation estimates at fine scales. J. Hydrometeor 8, 38–55. http://dx.doi.org/10.1175/JHM560.1.

Kasibhatla, P., Chameides, W.L., St John, J., 1997. A three-dimensional global model investigation of seasonal variation in the atmospheric Burden of anthropogenic sulfate aerosols. J. Geophys. Res. 102, 3737–3759. http://dx.doi.org/10.1029/96JD03084.

Kessler, E., 1969. On the distribution and continuity of water substance in atmospheric circulations. In: Meteorol. Monogr, vol. 32. Am. Meteorol. Soc., Boston, Mass, p. 84.

Kumar, P., Sokolik, I.N., Nenes, A., 2009. Parameterization of cloud droplet formation for global and regional models: including adsorption activation from insoluble CCN. Atmos. Chem. Phys. 9, 2517–2532.

Kuhlmann, J., Quaas, J., 2010. How can aerosols affect the Asian summer monsoon? Assessment during three consecutive pre-monsoon seasons from CALIPSO satellite data. Atmos. Chem. Phys. 10, 4673–4688. http://dx.doi.org/10.5194/acp-10-4673-2010.

Lau, K.-M., Kim, K.-M., 2006. Observational relationships between aerosol and Asian monsoon rainfall, and circulation. Geophys. Res. Lett. 33, L21810. http://dx.doi.org/10.1029/2006GL027546.

Lei, Y., Zhang, Q., He, K.B., Streets, D.G., 2011. Primary anthropogenic aerosol emission trends for China, 1990–2005. Atmos. Chem. Phys. 11, 931–954. http://dx.doi.org/10.5194/acp-11-931-2011.

Li, F.Y., Collins, W.D., Wehner, M.F., Williamson, D.L., Olson, J.G., Algieri, C., 2011. Impact of horizontal resolution on simulation of precipitation extremes in an aqua-planet version of Community Atmospheric Model (CAM3). Tellus A 63, 884–892. http://dx.doi.org/10.1111/J.1600-0870.2011.00544.X.

Lim, K.-S.S., Fan, J., Leung, L.R., Ma, P.-L., Singh, B., Zhao, C., Zhang, Y., Zhang, G., Song, X., 2014. Investigation of aerosol indirect effects using a cumulus microphysics parameterization in a regional climate model. J. Geophys. Res. Atmos. 119, 906–926. http://dx.doi.org/10.1002/2013JD020958.

Lin, Y.-L., Farley, R.D., Orville, H.D., 1983. Bulk parameterization of the snow field in a cloud model. J. Clim. Appl. Meteor. 22, 1065–1092. http://dx.doi.org/10.1175/1520-0450(1983)022<1065:BPOTSF>2.0.CO;2.

Liu, X., Easter, R.C., Ghan, S.J., Zaveri, R., Rasch, P., Shi, X., Lamarque, J.-F., Gettelman, A., Morrison, H., Vitt, F., Conley, A., Park, S., Neale, R., Hannay, C., Ekman, A.M.L., Hess, P., Mahowald, N., Collins, W., Iacono, M.J., Bretherton, C.S., Flanner, M.G., Mitchell, D., 2012. Toward a minimal representation of aerosols in climate models: description and evaluation in the Community Atmosphere Model CAM5. Geosci. Model Dev. 5, 709–739. http://dx.doi.org/10.5194/Gmd-5-

709-2012.
Liu, Y., Sun, J., Yang, B., 2009. The effects of black carbon and sulphate aerosols in China regions on East Asia monsoons. Tellus B 61, 642–656. http://dx.doi.org/10.1111/j.1600-0889.2009.00427.x.
Ma, P.-L., Rasch, P.J., Fast, J.D., Easter, R.C., Gustafson, W.I., Liu, X., Ghan, S.J., Singh, B., 2013. Assessing the CAM5 physics suite in the WRF Model: model implementation, evaluation, and resolution sensitivity. Geosci. Model Dev. Discuss. 6, 6157–6218. http://dx.doi.org/10.5194/gmdd-6-6157-2013.
Morrison, H., Gettelman, A., 2008. A new two-moment bulk stratiform cloud microphysics scheme in the Community Atmospheric Model (CAM3), Part I: description and numerical tests. J. Clim. 21, 3642–3659. http://dx.doi.org/10.1175/2008JCLI2105.1.
Mujumdar, M., Preethi, B., Sabin, T.P., Ashok, K., Saeed, S., Pai, D.S., Krishnan, R., 2012. The Asian summer monsoon response to the La Niña event of 2010. Met. Apps 19, 216–225. http://dx.doi.org/10.1002/met.1301.
Neale, R.B., et al., 2010. Description of the NCAR Community Atmosphere Model (CAM5.0). NCAR/TN-486+STR, NCAR, Boulder, Colo. Available at: http://www.cesm.ucar.edu/models/cesm1.0/cam/docs/description/cam5_desc.pdf.
Ohara, T., Akimoto, H., Kurokawa, J., Horii, N., Yamaji, K., Yan, X., Hayasaka, T., 2007. An Asian emission inventory of anthropogenic emission sources for the period 1980–2020. Atmos. Chem. Phys. 7, 4419–4444. http://dx.doi.org/10.5194/acp-7-4419-2007.
Park, S., Bretherton, C.S., 2009. The University of Washington shallow convection and moist turbulence schemes and their impact on climate simulations with the Community Atmosphere Model. J. Clim. 22, 3449–3469. http://dx.doi.org/10.1175/2008JCLI2557.1.
Qian, Y., Giorgi, F., 1999. Interactive coupling of regional climate and sulfate aerosol models over eastern Asia. J. Geophys. Res. 104, 6477–6499. http://dx.doi.org/10.1029/98JD02347.
Qian, Y., Giorgi, F., Huang, Y., Chameides, W.L., Luo, C., 2001. Regional simulation of anthropogenic sulfur over East Asia and its sensitivity to model parameters. Tellus 53B, 171–191. http://dx.doi.org/10.1034/j.1600-0889.2001.d01-14.x.
Qian, Y., Gong, D., Fan, J., Leung, L.R., Bennartz, R., Chen, D., Wang, W., 2009. Heavy pollution suppresses light rain in China: observations and modeling. J. Geophys. Res. 114, D00K02. http://dx.doi.org/10.1029/2008JD011575.
Rasch, P.J., Kristjansson, J.E., 1998. A comparison of the CCM3 model climate using diagnosed and predicted condensate parameterizations. J. Clim. 11, 1587–1614. http://dx.doi.org/10.1175/1520-0442(1998)011<1587:ACOTCM>2.0.CO;2.
Rasch, P.J., Mahowald, N.M., Eaton, B.E., 1997. Representations of transport, convection, and the hydrologic cycle in chemical transport models: implications for the modeling of short-lived and soluble species. J. Geophys. Res. 102, 28. http://dx.doi.org/10.1029/97JD02087, 127–28 138.
Remer, L.A., Kaufman, Y.J., Tanré, D., Mattoo, S., Chu, D.A., Martins, J.V., Li, R.-R., Ichoku, C., Levy, R.C., Kleidman, R.G., Eck, T.F., Vermote, E., Holben, B.N., 2005. The MODIS aerosol algorithm, products, and validation. J. Atmos. Sci. 62, 947–973. http://dx.doi.org/10.1175/JAS3385.1.
Schell, B., Ackermann, I.J., Hass, H., Binkowski, F.S., Ebel, A., 2001. Modeling the formation of secondary organic aerosol within a comprehensive air quality model system. J. Geophys. Res. 106, 28,275–28,293. http://dx.doi.org/10.1029/2001JD000384.
Seigneur, C., Pun, B., Pai, P., Louis, J.F., Solomon, P., Emery, C., Morris, R., Zahniser, M., Worsnop, D., Koutrakis, P., White, W., Tombach, I., 2000. Guidance for the performance evaluation of three-dimensional air quality modeling systems for particulate matter and visibility. J. Waste Manag. Assoc. 50, 588–599. http://dx.doi.org/10.1080/10473289.2000.10464036.
Song, X., Zhang, G.J., 2011. Microphysics parameterization for convective clouds in a global climate model: description and single column model tests. J. Geophys. Res. 116, D02201. http://dx.doi.org/10.1029/2010JD014833.
Stockwell, W.R., Middleton, P., Chang, J.S., Tang, X., 1990. The second generation regional acid deposition model chemical mechanism for regional air quality modeling. J. Geophys. Res. 95, 16,343–16,367. http://dx.doi.org/10.1029/JD095iD10p16343.
Stowe, L.L., Ignatov, A.M., Singh, R.R., 1997. Development, validation, and potential enhancements to the second-generation operational aerosol product at the national environmental satellite, data, and information service of the national oceanic and atmospheric administration. J. Geophys. Res. 102, 16. http://dx.doi.org/10.1029/96JD02132, 889–16 910.
Tan, J., Zhang, Y., Ma, W., Yu, Q., Wang, J., Chen, L., 2015. Impact of spatial resolution on air quality simulation: a case study in a highly industrialized area in Shanghai, China. Atmos. Pollut. Res. 6, 322–333. http://dx.doi.org/10.5094/APR.2015.036.
Tan, Q., Huang, Y., Chameides, W.L., 2002. Budget and export of anthropogenic SOx from east Asia during continental outflow conditions. J. Geophys. Res. 107 (D13), 4167. http://dx.doi.org/10.1029/2001JD000769.
U.S. EPA, 2001. Guidance for Demonstrating Attainment of Air Quality Goals for PM2.5 and Regional Haze. Draft 2.1, 2 January. The US Environmental Protection Agency, Office of Air and Radiation/Office of Air Quality Planning and Standards, Research Triangle Park, NC.
U.S. EPA, 2005. Guidance on the Use of Models and Other Analyses in Attainment Demonstrations for the 8-hour Ozone NAAQS. Draft Final Report, EPA-454/R-99–9004, 17 February. The US Environmental Protection Agency, Office of Air and Radiation/Office of Air Quality Planning and Standards, Research Triangle Park, NC.
Wang, J., Feng, J.M., Wu, Q.Z., Yan, Z.W., 2016. Impact of anthropogenic aerosols on summer precipitation in the Beijing–Tianjin–Hebei urban agglomeration in China: regional climate modeling using WRF-Chem. Adv. Atmos. Sci. 33 (6), 753–766. http://dx.doi.org/10.1007/s00376-015-5103-x.
Wang, K., Zhang, Y., Zhang, X., Fan, J.-W., Leung, L.R., Zhang, Q., He, K.-B., 2017. Fine scale application of WRF-CAM5: sensitivity of aerosol indirect effects to aerosol activation parameterization and grid resolution. Atmos. Environ. in review.
Wu, T., Yu, R., Zhang, F., 2008. A modified dynamic framework for the atmospheric spectral model and its application. J. Atmos. Sci. 65, 2235–2253.
Wu, L., Su, H., Jiang, J.H., 2013. Regional simulation of aerosol impacts on precipitation during the East Asian summer monsoon. J. Geophys. Res. Atmos. 118, 6454–6467. http://dx.doi.org/10.1002/jgrd.50527.
Xu, J., Bergin, M.H., Yu, X., Liu, G., Zhao, J., Carrico, C.M., Baumann, K., 2002. Measurement of aerosol chemical, physical and radiative properties in the Yangtze Delta region of China. Atmos. Environ. 36, 161–173. http://dx.doi.org/10.1016/S1352-2310(01)00455-1.
Yahya, K., Glotfelty, T., Wang, K., Zhang, Y., Nenes, A., 2017. Modeling regional air quality and climate: improving organic aerosol and aerosol activation processes in WRF/Chem version 3.7.1. Geosci. Model Dev. 10, 2333–2363. http://dx.doi.org/10.5194/gmd-10-2333-2017.
Yihui, D., Chan, J.C.L., 2005. The East Asian summer monsoon: an overview. Meteorol. Atmos. Phys. 89, 117–142. http://dx.doi.org/10.1007/s00703-005-0125-z.
Zaveri, R.A., Peters, L.K., 1999. A new lumped structure photochemical mechanism for large-scale applications. J. Geophys. Res. 104 (D23), 30,387–30,415. http://dx.doi.org/10.1029/1999JD900876.
Zender, C.S., Bian, H.S., Newman, D., 2003. Mineral dust entrainment and deposition (DEAD) model: description and 1990s dust climatology. J. Geophys. Res. Atmos. 108 http://dx.doi.org/10.1029/2002JD002775.
Zhang, G.J., McFarlane, N.A., 1995. Sensitivity of climate simulations to the parameterization of cumulus convection in the canadian climate centre general circulation model. Atmos. Ocean. 33, 407–446. http://dx.doi.org/10.1080/07055900.1995.9649539.
Zhang, G.J., Mu, M., 2005. Effects of modifications to the Zhang-McFarlane convection parameterization on the simulation of the tropical precipitation in the national center for atmospheric Research community climate model, version 3. J. Geophys Res. 110 http://dx.doi.org/10.1029/2004JD005617.
Zhang, H., Wang, Z., Wang, Z., Liu, Q., Gong, S., Zhang, X., Shen, Z., Lu, P., Wei, X., Che, H., Li, L., 2012. Simulation of direct radiative forcing of aerosols and their effects on East Asian climate using an interactive AGCM-aerosol coupled system. Clim. Dyn. 38, 1675–1693. http://dx.doi.org/10.1007/s00382-011-1131-0.
Zhang, M., Lin, W., Bretherton, C.S., Hack, J.J., Rasch, P.J., 2003. A modified formulation of fractional stratiform condensation rate in the NCAR community atmospheric model CAM2. J. Geophys. Res. 108 http://dx.doi.org/10.1029/2002JD002523.
Zhang, Q., Streets, D.G., Carmichael, G.R., He, K.B., Huo, H., Kannari, A., Klimont, Z., Park, I.S., Reddy, S., Fu, J.S., Chen, D., Duan, L., Lei, Y., Wang, L.T., Yao, Z.L., 2009. Asian emissions in 2006 for the NASA INTEX-B mission. Atmos. Chem. Phys. 9, 5131–5153. http://dx.doi.org/10.5194/acp-9-5131-2009.
Zhang, Y., Liu, P., Pun, B., Seigneur, C., 2006a. A comprehensive performance evaluation of MM5-CMAQ for summer 1999 southern oxidants study episode, Part-I. Evaluation protocols, databases and meteorological predictions. Atmos. Environ. 40, 4825–4838.
Zhang, Y., Liu, P., Queen, A., Misenis, C., Pun, B., Seigneur, C., Wu, S.-Y., 2006b. A comprehensive performance evaluation of MM5-CMAQ for summer 1999 southern oxidants study episode, part-II. Gas and aerosol predictions. Atmos. Environ. 40, 4839–4855.
Zhang, X., 2013. Examining Aerosol Indirect Effects Using a Regional Climate-aerosol Model with Improved Aerosol Activation and Cloud Parameterizations. Thesis submitted to Graduate Faculty of North Carolina State University, Raleigh, NC.
Zhang, Y., Zhang, X., Wang, K., He, J., Leung, L.R., Fan, J., Nenes, A., 2015. Incorporating an advanced aerosol activation parameterization into WRF-CAM5: model evaluation and parameterization intercomparison. J. Geophys. Res. Atmos. 120, 6952–6979. http://dx.doi.org/10.1002/2014JD023051.
Zheng, Y., Alapaty, K., Herwehe, J.A., Del Genio, A.D., Niyogi, D., 2016. Improving high-resolution weather forecasts using the weather Research and forecasting (WRF) model with an updated Kain–fritsch scheme. Mon. Wea. Rev. 144, 833–860. http://dx.doi.org/10.1175/MWR-D-15-0005.1.
Zhu, J., Liao, H., Li, J., 2012. Increases in aerosol concentrations over eastern China due to the decadal-scale weakening of the East Asian summer monsoon. Geophys. Res. Lett. 39, L09809. http://dx.doi.org/10.1029/2012GL051428.